7.125

Simulation Of Mono And Dual-Wavelength Airborne Radar Observations Of Precipitating Systems At Various Frequency Bands

V. Louf[1]*, O. Pujol[1], H. Sauvageot[2], J. Riedi[1], and G. Pénide[1]
[1]Université Lille 1, Laboratoire d'Optique Atmosphérique (LOA);
[2]Université Toulouse III, Observatoire Midi-Pyrénées.

1. Introduction

We address the question of the most efficient couple (f, θ_{3dB}) for airborne radar precipitating system observations, where f is the microwave frequency and θ_{3dB} the beamwidth aperture at 3 dB ($\theta_{3dB} = 70\lambda/D_a$, D_a is antenna diameter) (Skolnik 2008). This problem is of importance. The meteorological hazard in civil aviation is mainly due to convective precipitating systems, and particularly hail and strong turbulence areas.

A realistic and flexible model of precipitating systems is presented and simulations of airborne radar observations are performed at the six meteorological frequency bands. In this work, the effect of f and θ_{3dB} modification is shown through radar simulations of several precipitating systems. One is a numerical simulation composed of two successive rows of convective towers, another is inspired from NEXRAD data of a real mesoscale event of May 2[nd], 2003 in Alabama (USA), presenting hail-bearing convective towers. It is shown that some (f, θ_{3dB}) couples are better than the one currently used by civil aviation. Notably C-band allows a better description than X-band of a meteorological radar scene, if the radar antenna size is increased.

After that, we applied the dual-wavelength method to detect unambiguously hail in these precipitating systems. The question of the most efficient dual-wavelength couple is addressed by comparing several meteorological radar dual-bands. Since hail reflectivity is strongly dependent on microwave frequency (Atlas and Ludlam 1961), an interesting method to improve hail detection in airborne radar is the dual-wavelength technique (DWT). As a non-Rayleigh scatterer at S, C, and X-bands, hail reflectivity field is considerably higher as the frequency decreases. It is shown that even if S-X is the best couple, because the reflectivity difference is the highest, C-X is a dual-wavelength of interest. It is also shown that, because of the non-Rayleigh scattering behavior of hailstones, the derivative of the dual-wavelength reflectivity ratio is a tool that can unambiguously detect hail on the radar signal path.

*Corresponding author address: Valentin Louf, Université Lille 1, Laboratoire d'Optique Atmosphérique, 59655 Villeneuve d'Ascq, France; e-mail: valentin.louf@ed.univ-lille1.fr

2. Method

Simulation of precipitating system observations are made using the method described in detail in Louf et al. (2013). Briefly, it consists in modeling a mesoscale precipitating system with several convective towers surrounded by a stratiform background (Houze 1997). This system is composed of nine hydrometeor categories (rain, dry and wet hail, dry and wet snow, graupel, drizzle, ice crystals, and water droplets), each one being characterized by a three-dimensional concentration field and a size spectrum distribution.

Observations are simulated for an airborne radar located on a plane flying at 10 km of altitude which operates at the six meteorological frequencies $S\,(f \approx 3\,\mathrm{GHz}, \lambda \approx 10.7\,\mathrm{cm})$, $C\,(f \approx 5.5\,\mathrm{GHz}, \lambda \approx 5.5\,\mathrm{cm})$, $X\,(f \approx 9.4\,\mathrm{GHz}, \lambda \approx 3.2\,\mathrm{cm})$, $K_u\,(f \approx 15\,\mathrm{GHz}, \lambda \approx 2\,\mathrm{cm})$, $K_a\,(f \approx 35\,\mathrm{GHz}, \lambda \approx 0.86\,\mathrm{cm})$, and $W\,(f \approx 94\,\mathrm{GHz}, \lambda \approx 0.32\,\mathrm{cm})$. Range bin spacing Δr is set to 150 m. Electromagnetic energy is supposed to be uniformly distributed

The size distribution of each hydrometeor category is required to compute the reflectivity fields, and thus, a complete modeling of the target microphysics is needed (Pruppacher and Klett 1997). The detail for all hydrometeor categories can be found in Louf et al. (2013). Equivalent radar reflectivity factor and attenuation are then computed from backscattering (σ) and attenuation (Q) cross sections of spherical scatterers given by Mie formulas. For a given radar cell of volume $\mathcal{V}$, the procedure consists in identifying the grid points included in $\mathcal{V}$ and, for each of these grid points, to compute σ and Q at the considered microwave frequency. The equivalent radar reflectivity factor of $\mathcal{V}$ is finally calculated with the Probert-Jones (1962) equation. The simulation is fully completed when the successive radar beams separated by $\Delta\theta = 0.1°$ in azimuth have covered the whole extent of the target.

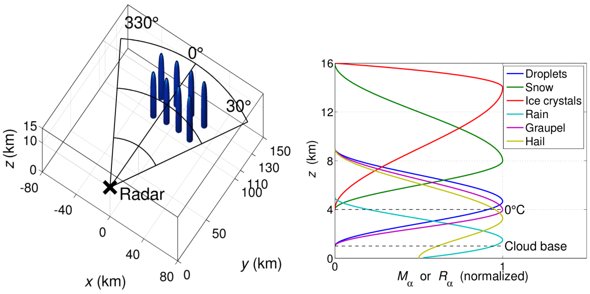

Figure 1: (a) Numerical model configuration. Radar is located at $(0, 0, 10)$, range markers are circumscribing every $50\,\mathrm{km}$. The cell center of the first row of convective tower is at $110\,\mathrm{km}$ from the radar and the second at $130\,\mathrm{km}$. The towers have circular horizontal section with diameter of $10\,\mathrm{km}$. (b) Normalized vertical profile of hydrometeors in a convective tower. For the hydrometeor category α, M_α is the water content and R_α the precipitation rate.

3. Frequency and $\theta_{3\mathrm{dB}}$-beamwidth comparison

Figure 2 shows a PPI view of the simulated Z_m-field at the six frequency bands of a plane flying along azimuth direction $0°$, at $10\,\mathrm{km}$ of altitude. Z_m-field degradation is clearly visible. At S and C-bands (Fig. 2a, b), although the large $\theta_{3\mathrm{dB}}$ beamwidths do not permit to isolate each convective towers, two lines of convection of reflectivity greater than $50\,\mathrm{dBZ}$ are clearly visible. At $X-$band (Fig. 2c), only the first row of convection is seen with the correct range of reflectivity while the second row is attenuated. The farthest one does not seem to be dangerous: reflectivity falls down of $15\,\mathrm{dB}$ because of attenuation. Attenuation is worse for the highest frequency bands, i.e. at K_u (Fig. 2d), K_a (Fig. 2e), and W (Fig. 2f) bands, for which the convective system is clearly unobservable. These three bands are not appropriate for hail and/or high rainfall detection. They are not interesting for meteorological hazard estimation, although these microwaves propagate with a narrow beam in spite of small radar antenna.

The same conclusion holds for an RHI view, like that presented on Fig. 3 for an azimuth of $0°$, i.e. with a perfect alignment of the radar with the two centered convective cells. The cumulonimbus are easily identifiable at S, C, and X-bands (Fig. 3a, b, and c respectively), despite the large $\theta_{3\mathrm{dB}}$-beamwidths used. However, attenuation destroys the possibility to observe unambiguously these two convective towers at K_u, K_a, and W-bands (Fig. 3d, e, and f).

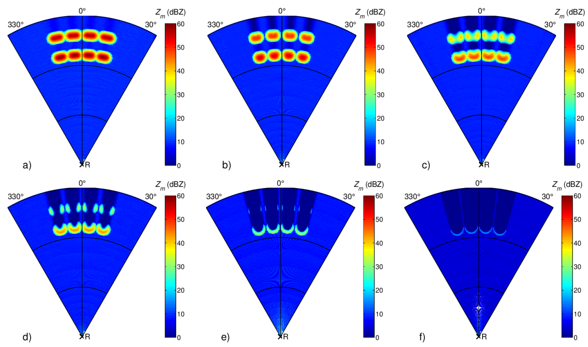

Figure 2: Simulation of a PPI view (altitude $10\,\mathrm{km}$) of $Z_m(\,\mathrm{dBZ})$, at: S(a), C(b), X(c), K_u(d), K_a(e), and W(f). Radar antenna diameter is $200\,\mathrm{cm}$ (a, b) and $80\,\mathrm{cm}$ (c, d, e, f). R indicates radar position. Range markers are as in Fig. 1a.

In order to study the angular resolution effect, several others simulations have been performed. Radar antenna diameter has been changed. On Figure 4a, b, and c, radar antenna diameter is $2\,\mathrm{m}$ for all three bands. The corresponding angular resolutions are $\theta_{3\,\mathrm{dB}} = 3.7°$ for S-band, $1.9°$ for C-band, and $1.1°$ for X-band. Compared to Figure 2, there is no substantial change for S and C-bands. However, $X-$band presents a good improvement (Fig. 4c), since the eight convective towers seems to be quite well separated. In addition, they appear to be less attenuated than in Figure 2, since the radar resolution volume has been decreased.

Fig. 4d, e, and f the radar antenna diameter is $4\,\mathrm{m}$, which gives $\theta_{3\mathrm{dB}}$-beamwidths of $1.9°$, $0.9°$, and $0.5°$ at S, C, and X-bands respectively. All the convective towers are clearly identifiable at X and $C-$bands. At $S-$band, only the second convective

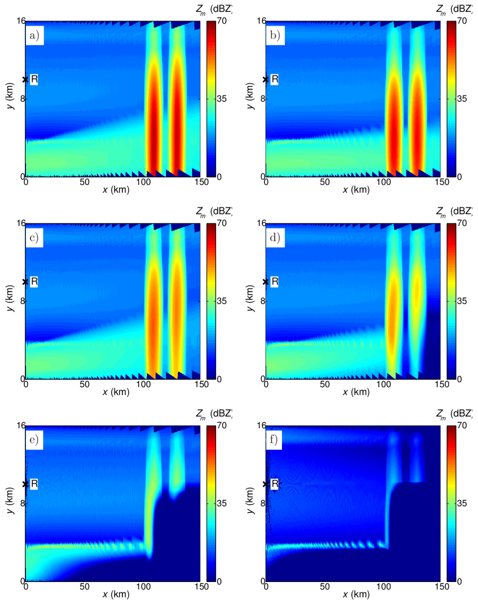

Figure 3: Idem as Fig. 2 but for a RHI view of azimuth 0°..

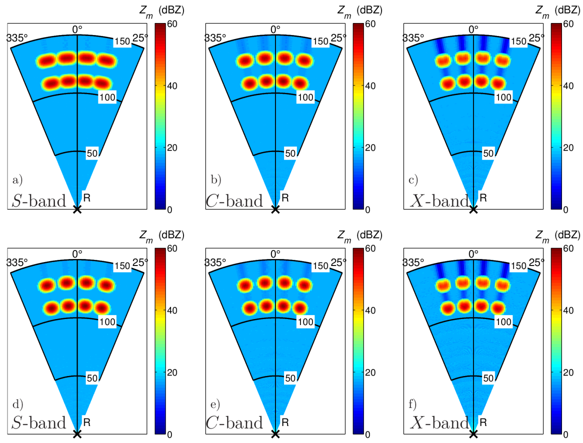

Figure 4: PPI view simulation of the measured reflectivity $Z_m(\,\mathrm{dBZ})$ in a mesoscale system at various frequency bands: S(a,d), C(b,e), X(c,f), with a radar antenna size of $2\,\mathrm{m}$ (a,b,c) and of $4\,\mathrm{m}$ (d,e,f).

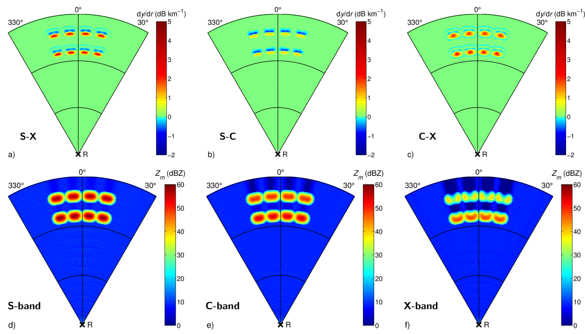

Figure 5: PPI field of $\mathrm{d}y/\mathrm{d}r$ for the frequency couples $S-X$ (a), $S-C$ (b), and $C-X$ (c). PPI field of measured reflectivity in S (d), C (e), and X-bands (f).

line does not show a succession of four towers. For these three frequency bands, increasing diameter improves the quality of the information given by the radar.

4. Dual-wavelength technique

The use of the reflectivity dependence on the wavelength in the Mie scattering region to distinguish hail from rain using simultaneous observations with a ground-based dual-wavelength radar was first proposed by Atlas and Ludlam (1961). Eccles and Atlas (1973) have reformulated the dual-wavelength approach and proposed a method using the range derivative of the dual wavelength ratio (DWR):

$$\frac{\mathrm{d}y}{\mathrm{d}r} = \frac{\mathrm{d}}{\mathrm{d}r}[Z_{m,\lambda_l}(r) - Z_{m,\lambda_s}(r)] \qquad (1)$$

where Z_m is the measured reflectivity at a wavelength λ (l for large and s for small). Note that hail is the only non-Rayleigh meteorological scatterer at S-band.

In addition, hail is the only hydrometeor to present a significant reflectivity difference at S, C, and X-bands. Different studies have confirmed the relevance of the $S-C$, $C-X$, and $S-X$ frequency couples for meteorological observations. For instance, Féral et al. (2003) have used the radar reflectivity difference between S and C-bands to identify hailstorms in various convective conditions from non-collocated ground-based radars.

These simulations suggest using $\mathrm{d}y/\mathrm{d}r$ to detect convective cells containing hail. The front of a hail area has a strong positive variation, while the rear is negative. To delimit completely a hail area, the measured reflectivity is a significant complementary information. Indeed, on Figure 5, which shows $\mathrm{d}y/\mathrm{d}r$ for $S-X$, $S-C$, and $C-X$ frequency couples (Figs. 5a, b, c) and the measured reflectivity Z_m at S, C, and X-bands (Figs. 5d, e, f) for dry hail, one observes high positive values of $\mathrm{d}y/\mathrm{d}r$ at the front of hail cells and negative values of $\mathrm{d}y/\mathrm{d}r$ (between -0.5 and $-1\,\mathrm{dB\,km^{-1}}$) at the rear side. Thus $\mathrm{d}y/\mathrm{d}r$ associated with high Z_m-values enable to delimit the corresponding convective cells and hail areas.

In order to illustrate the usefulness of the dual-wavelength ratio to determine hail areas, let consider a real mesoscale precipitating system that occurs on May 2003, 2nd in Alabama (USA). The radial derivative of the reflectivity difference, $\mathrm{d}y/\mathrm{d}r$, is considered (Figs. 6a, b, c). Associated with the measured reflectivity (Figs. 6d, e, f), hail areas for this real case are clearly localized. The frequency couples $S-X$ and $C-X$ (Figs. 6a, c) are the best ones, with Z_m-values (higher than $50\,\mathrm{dBZ}$) at S and C-bands (Figs. 6d, e).

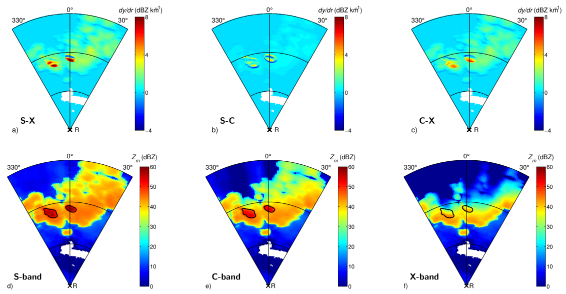

Figure 6: PPI field simulation of $\mathrm{d}y/\mathrm{d}r$ of real hailstorm for the frequency couples $S-X$ (a), $S-C$ (b), and $C-X$ (c). PPI field of measured reflectivity in dBZ at S (d), C (e), and X-bands (f). Black contours delimit hail areas. Range markers are as in Fig. 1a. Blank area between 30 and $50\,\mathrm{km}$ is due to a lack of data.

5. Conclusion

We have studied the effect of different parameters: f, $\theta_{3\mathrm{dB}}$, rainfall and hailfall rate, and dual-wavelength configuration. For this, more than 400 systems (numerical or inspired from a real case) have been computed. Due to the relation $\theta_{3\mathrm{dB}} = 70\lambda/D$, decreasing $\theta_{3\mathrm{dB}}$ implies decreasing λ or increasing D. The simulation presented herein on modeled precipitating systems, (numerical or inspired from real ones) with $D = 2\,\mathrm{m}$ or $4\,\mathrm{m}$, shows that (1) S-band is the best one to distinguish hail from rain since it does not suffer microwave attenuation, but a low $\theta_{3\mathrm{dB}}$-values implies using an important antenna diameter; (2) $X-$band is penalized by attenuation, but allows quite good $\theta_{3\mathrm{dB}}$-resolution; (3) $C-$band seems to be a good compromise between antenna diameter, a relatively low attenuation, and the necessity to identify the meteorological hazard far enough from the radar $(150\,\mathrm{km})$.

Such comparative study between various microwave frequencies has never been made for an airborne radar in the frame of civil aviation. In addition, on the context of airborne radar for civil aviation the literature is not so rich, to that about ground-based meteorological radar observations. Rather, one can find many patents about the former topic.

Acknowledgement The authors are indebted to the US NOAA/National Weather Service for providing without any charge the excellent NEXRAD network radar data used for this work.

References

Atlas, D. and F. H. Ludlam, 1961: Multi-wavelength radar reflectivity of hailstorms. *Quart. J. Roy. Meteorol. Soc.*, **87**, 523–534, doi:10.1002/qj.49708737407.

Eccles, P. J. and D. Atlas, 1973: A Dual-Wavelength Radar Hail Detector. *J. Appl. Meteorol.*, **12**, 847–854.

Féral, L., H. Sauvageot, and S. Soula, 2003: Hail Detection Using S- and C-Band Radar Reflectivity. *Journal of Atmospheric and Oceanic Technology*, **20**, 233–248.

Houze, R. A., 1997: Stratiform precipitation in regions of convection: A meteorological paradox? *Bulletin of the American Meteorological Society*, **78**, 2179–2196.

Louf, V., O. Pujol, H. Sauvageot, and J. Riedi, 2013: Simulation of airborne radar observations of precipitating systems at various frequency bands. *Geoscience and Remote Sensing, IEEE Transactions on (in press)*, doi:10.1109/TGRS.2013.2252910.

Probert-Jones, J. R., 1962: The radar equation in meteorology. *Q. J. R. Meteor. Soc.*, **88**, 485–495.

Pruppacher, H. R. and J. D. Klett, 1997: *Microphysics of clouds and precipitation*. Atmospheric and oceanographic sciences library, Kluwer Academic Publishers, 976 pp.

Skolnik, M., 2008: *Radar Handbook, Third Edition*. Electronics electrical engineering, McGraw-Hill.